Evaluation of the counterion distribution around spherical micelles in solution by small-angle neutron scattering

Kimio Sumaru, Hideki Matsuoka, and Hitoshi Yamaoka*
Department of Polymer Chemistry, Kyoto University, Kyoto 606-01, Japan

George D. Wignall
Neutron Scattering Group, Solid State Division, Oak Ridge National Laboratory, P.O. Box 2008, Oak Ridge, Tennessee 37831
(Received 6 July 1995)

The counterion distribution around tetramethylammonium dodecyl sulfate micelles has been evaluated by small-angle neutron scattering (SANS) using the contrast variation technique. The scattering from the counterions and the hydrated shell was isolated by matching the scattering length densities of the core and aqueous medium by adjusting the H_2O-to-D_2O ratio. Thus the core component of the scattering was "erased," due to zero contrast with the solvent. The counterion distribution was estimated by fitting the SANS data to a model of an isolated particle consisting of a core, shell, and counterion atmosphere, with only three adjustable parameters. For a micellar concentration of 6 vol %, the aggregation number, core radius, shell thickness, and charge number were estimated as 77, 18.6 Å, 4.6 Å, and 44, respectively. Similar values were obtained for a concentration of 3 vol %. In addition, the electrostatic potential and the dissociation equilibrium at the micellar surface were also evaluated. The estimated value of the surface potential of micelles ($-4.7kT$) indicated the validity of using the numerical solution of nonlinear Poisson-Boltzmann equation for the calculation of the counterion distribution.

PACS number(s): 82.70.Kj, 61.12.Ex

I. INTRODUCTION

The electrostatic potential plays a fundamental role in determining the properties of macroionic systems such as a polyelectrolyte and ionic micellar solutions, in view of the strength and extended range of the interaction. The distribution of ions and counterions, on which the strength and the range of the electrostatic interaction greatly depend, is one of the most important factors that influence the characteristics of such systems. Thus many studies on this problem have been undertaken in a variety of macroion geometries including linear [1–7], spherical [1,8–14], and planar [15,16] macroionic systems. For lightly charged systems, the counterion distribution is well described by linear approximation theories [17], which can be used to describe the characteristics such as osmotic coefficient and activity in highly charged systems. However, it is virtually impossible to treat the counterion distribution near the surface of the macroion (i.e., the condensed region) analytically because of the extreme heterogeneity of the electrostatic potential in the system [18]. In addition, no effective method to determine the whole profile of the counterion distribution has been proposed so far. Data obtained by the other methods such as potentiometry, osmosis, electrophoresis, and viscoelastic measurement contain no direct information on the geometrical organization of the system. Small-angle neutron scattering (SANS) data are measured as a function of the scattering vector and thus contain information on the spatial distribution of ions. Thus SANS data can, in principle, provide important information on the counterion distribution, as a function of the distance from the center of a micelle. Furthermore, by means of contrast variation methods, it is possible to isolate the scattering from the counterions. Wu *et al.* [19,20] carried out the small-angle x-ray scattering and SANS measurements for cylindrical micellar solution in order to evaluate the counterion distribution. However, the charge density was *defined* stoichiometrically from the amount of the ionic surfactant and was not determined from the scattering data. More recently, van der Maarel *et al.* [21] evaluated the counterion distribution in tetramethylammonium polystyrenesulfonate solutions as linear macroionic systems by SANS based on the assumption that the systems consist of randomly oriented cylinders [21]. For the spherical macroionic systems, however, the atmospheric distribution of counterions have never been taken into account, as far as we know, although SANS analyses for the various kinds of ionic micellar solutions have been performed to estimate intra- and intermicellar structures [22–27].

In this study, SANS measurements were carried out to determine the counterion distribution around highly charged spherical micelles. The advantage of the system studied in this work is that the micellar system can be regarded as spherical to a good approximation and this enables us to analyze the data quantitatively without resorting to additional assumptions. Although the small-angle scattering from counterions is generally weak, it may be enhanced for SANS by deuterium labeling of both the solvent and solute micelles. In this study, we used dodecylsulfate (DS) to form the micelle and hydrogenated (H_{12}) or deuterated (D_{12}) tetramethylammonium (TMA) as the counterion. SANS measurements were performed for both H_{12}-TMADS and D_{12}-TMADS solutions with three different D_2O-to-H_2O ratios to give a total of four

*Author to whom correspondence should be addressed.

 ©1996 The American Physical Society

different contrast conditions, which were used to extract the scattering from counterions. The scattering data from the differently contrasted micelles were all fitted by the same structural model of an isolated spherical micelle, composed of the hydrophobic core, hydrophilic shell, and counterion cloud. From the results, significant information was obtained on the counterion distribution, in addition to the structural parameters of the micelle (e.g., core and shell radii, aggregation number, etc.).

II. EXPERIMENT

A. Principle of contrast variation in SANS

In general, radiation incident on a medium whose scattering power is independent of position is scattered only into the forward direction (i.e., at zero angle). Scattering only occurs at finite angles if the scattering power of the medium fluctuates from point to point in the sample. Thus x-ray scattering is caused by fluctuations in electron density, whereas neutrons are deflected by fluctuations in scattering length density (SLD). Whereas all electrons have the same scattering amplitude, the equivalent quantity for neutrons (the scattering length) is specific to each atom (isotope). These are tabulated in standard reference work [28]. Interestingly, there is a large difference between the scattering lengths of H and D atoms, though to a good approximation their chemical behavior is similar. The scattering length of D is a large positive value while that of H is negative. This means that the neutron scattering power can be changed by D labeling either the solvent or solute. Such contrast variation techniques have been described in detail elsewhere [29,30]. We used H-dodecyl sulfate (H-DS) and H- and D-tetramethylammonium (H-TMA and D-TMA) in order to observe the scattering from counterions (internal contrast variation). We used mixtures of H_2O and D_2O as a solvent to *erase* the scattering from the core component of the micelle particle (external contrast variation) and also to enhance the scattering from the counterions. The combination of these internal and external contrast variation techniques made feasible the isolation of the scattering from counterions with high signal-to-noise ratio. The values of scattering length (summed over the atomic constituents) and SLD (ρ) calculated by dividing by the molar volume (v) ($\rho=\sum_i b_i/v$) are summarized in Table I.

TABLE I. Molecular volume (MV), scattering length, and scattering density of chemical species.

Species	MV (nm^3)	$\sum b$ (fm)	ρ (fm/nm^3)
$C_{12}H_{25}$	0.350	−13.741	−39
SO_4^-	0.0579	26.07	450
DS^-	0.408	12.33	30
$N(CH_3)_4^+$	0.140	−8.936	−64
$N(CD_3)_4^+$	0.140	116.04	829
H_2O	0.0299	−1.677	−56
D_2O	0.0302	19.153	634

B. Preparation of samples

D_{12}-TMADS was prepared as follows: sodium dodecyl sulfate [(SDS), Nacalai Tesque Inc., Kyoto, Japan] was dissolved in Milli-Q reagent grade water (Millipore, Bedford, MA) and was protonated completely into dodecylsulfuric acid (HDS) by using excess cation exchange resin AG-1-X8 (Bio-rad Laboratory, Richmond, CA). By comparison, tetramethyl D_{12} ammonium bromide (Euriso-Top, Gif-sur-Yvette, France) was also dissolved in Milli-Q water and treated with excess anion exchange resin AG-50W-X8 (Bio-rad Laboratory) to yield D_{12}-TMAOH solution. With small amount of HDS and D_{12}-TMAOH solutions, conductometric titration was carried out to determine the equivalence point by using a conductivity meter DS-8M (Horiba Ltd., Kyoto, Japan). Based on this result, the HDS solution was neutralized with an equivalent amount of D_{12}-TMA solution. After vigorous stirring, the mixed solution was freeze-dried and yielded D_{12}-TMADS as white powder. H_{12}-TMADS was also prepared using water-dissolved tetramethylammonium hydroxide pentahydrate [(H_{12}-TMAOH·$5H_2O$), Aldrich Chemical Company Inc., Milwaukee, WI] instead of the D_{12}-TMAOH solution. Series of solvents were prepared by mixing deuterium oxide [(D_2O), Uvasol grade, E. Merck, Darmstadt, Germany] and Milli-Q H_2O at the prescribed ratios.

Sample solutions of 6 and 3 vol % were prepared with D_{12}- and H_{12}-TMADS and D_2O-H_2O solvents in four different SLD contrasts at each volume fraction. In principle, isolated noninteracting micelles are observed only in the limit of an infinitely dilute solution. However, in order to achieve a measurable SANS cross section with a good signal-to-noise ratio, we employed these concentrations in which the micellar particles are electrostatically interacting with each other, as will be described below. The measurement conditions are summarized in Table II for four different contrast conditions (CCs 1–4). For CC 1, the solvent SLD (ρ) matched that of the hydrocarbon core ($C_{12}H_{25}$) of the micelle. Contrast conditions 2 and 3 refer to D_{12}-TMADS and H_{12}-TMADS, respectively, dissolved in pure D_2O. Contrast condition 4 refers to H_{12}-TMADS in a 17.4-vol % D_2O solvent. It will be seen subsequently that, although the counting statistics are not as good for this contrast condition, the data are consistent with the overall interpretation established from contrast conditions 1–3, thus providing a valuable complimentary cross-check on the analysis.

C. SANS measurements

The SANS data were collected on the W. C. Koehler 30-m SANS facility [31] at the Oak Ridge National Laboratory (ORNL) with a (64×64)-cm^2 area detector and cell (element) size approximately equal to 1 cm^2. The neutron wavelength was 4.75 Å ($\Delta\lambda/\lambda\sim5\%$) and the sample-detector distance was 2.4 m. The data were corrected for instrumental backgrounds and detector efficiency on a cell-by-cell basis, prior to radial averaging, to give a q range $0.025<q=4\pi\lambda^{-1}\sin\theta<0.25$ $Å^{-1}$, where $\lambda=4.75$ Å is the wavelength and 2θ is the angle of

TABLE II. Characteristics and fitted parameters for samples.

Concentration	CC			CSI model						CS model				
(vol %)	No.	ϕ_{D_2O}	Counterion	N	R_1 (Å)	R_2 (Å)	Z	w	φ_s	N	R_1 (Å)	R_2 (Å)	Z	w
6	1	0.024	D_{12}-TMA$^+$	77	18.6	23.2	44	7.0	−4.66	79	18.8	25.7	22	13.0
	2	1	D_{12}-TMA$^+$											
	3	1	H_{12}-TMA$^+$											
	4	0.174	H_{12}-TMA$^+$											
3	1	0.024	D_{12}-TMA$^+$	77	18.6	23.6	38	7.9	−4.61	75	18.4	25.0	21	16.9
	2	1	D_{12}-TMA$^+$											
	3	1	H_{12}-TMA$^+$											

scatter. The solutions were contained in quartz cells (2–5 mm path length) and the coherent intensities of the samples were obtained by subtracting the intensities of the corresponding cell, which formed only a minor correction (<2%) to the sample data. The net intensities were converted to an absolute (±3%) differential cross section [$I_{expt}(q)$] per unit sample volume (in units of cm^{-1}) by comparison with precalibrated standards, based on the measurement of beam flux, the vanadium incoherent cross section, and the scattering from water and other reference materials [32]. The efficiency calibration was based on the scattering from light water and this led to angle-independent scattering for vanadium, H-polymer blanks, and water samples of different thicknesses in the range 1–10 mm.

The transmission of the sample was measured in a separate experiment by collimating the beam with slits (irises) approximately equal to 1 cm in diameter, separated by a distance approximately 7.5 m. A strongly scattering sample, porous carbon, was placed at the sample position to spread the beam over the whole detector, placed at a sample-detector distance approximately equal to 10 m. Without the carbon in position, the beam would be either blocked by the beam stop or concentrated in a few detector cells, with the possibility of saturating or damaging the detector. The total count summed over the whole detector ($>10^5$) was recorded in a time period approximately equal to 1 min and the sample being measured was placed over the source slit, thus attenuating the beam. The count was repeated over the same time interval and the transmission is given by the ratio of the two counts after minor corrections (<0.1%) for the beam-blocked background due to electronic noise, cosmic rays, etc. In this geometry, only scattering from the same at q values less than 10^{-3} Å^{-1} can enter the second iris and be scattered by the porous carbon and hence be counted by the detector.

III. RESULTS

Figure 1 shows the SANS data from the 6% TMADS solutions at the three different contrast conditions (1–3) specified in Table II. For each condition, a single broad peak was observed, indicating the existence of a more or less ordered structure in the system arising from the strong electrostatic interaction between micellar particles. The profiles at contrast conditions 2 and 3 are at first sight very similar and the peak position is virtually the same. However, on close examination differences may be observed, especially at higher q values. The two curves intersect at $q \approx 0.14$ Å^{-1}, indicating subtle differences in the scattering length density profiles. A peak is also observed at CC 1, but the peak position is somewhat different from that observed where the contribution of the core is dominant (CCs 2 and 3). For CC 1, the SLD of the solvent was matched to that of the micel-

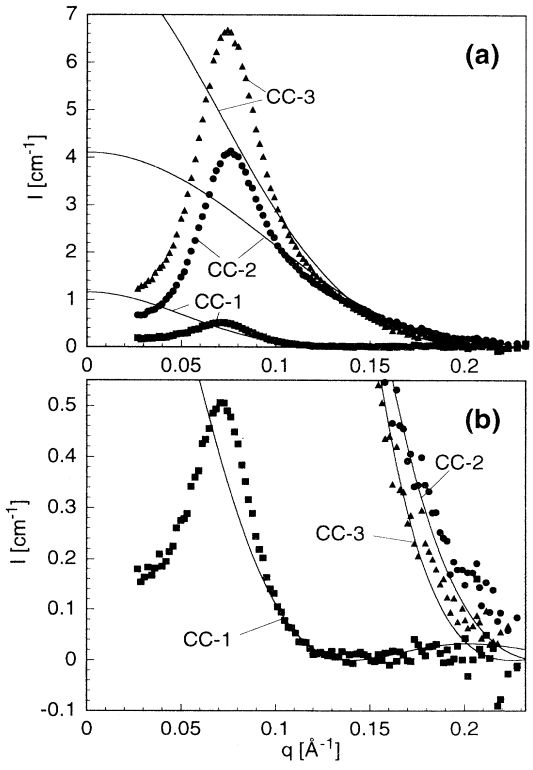

FIG. 1. $I_{expt}(q)$ (■, ●, and ▲) and $n_pP(q)$ (——, calculated with the CSI model) of 6-vol % samples at three contrast conditions (Table II) plotted against scattering vector q. (a) and (b) are different only in their I scale.

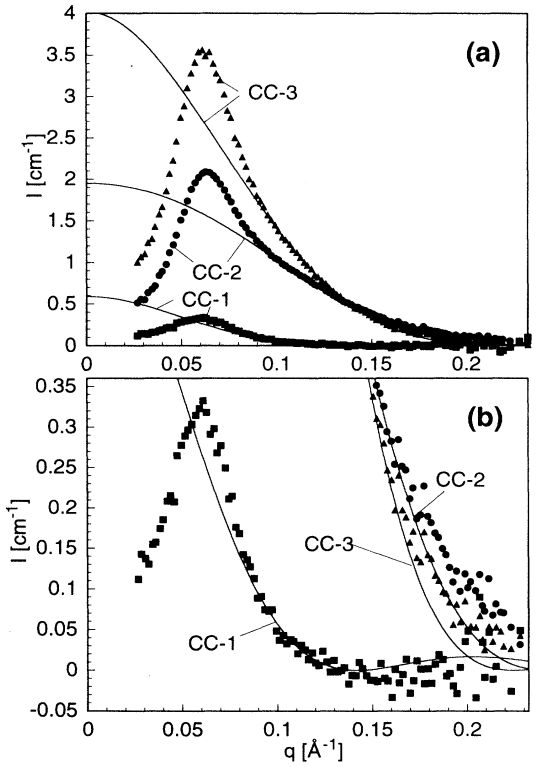

FIG. 2. $I_{expt}(q)$ and $n_pP(q)$ of 3-vol % samples at three contrast conditions plotted against q. Symbols are as in Fig. 1.

lar core. Hence the scattering is sensitive only to the shell and counterion parts of the micelle and this is the origin of the large difference of the SANS profile from contrast conditions 2 and 3.

Figure 2 shows SANS profiles for the samples with 3 vol % concentration. The general trends are similar to the previous observations, with the exception that the shift of the interference peak is less, due to the lower micellar concentration.

IV. DISCUSSION

A. Basic assumptions and scattering function for the analysis of SANS data

The SANS data were analyzed by fitting to a structural model based on the following assumptions.

(i) The molecular volumes and chemical properties of D_{12}- and H_{12}-TMA^+, D_2O, and H_2O are the same, apart from their molecular weight (specific gravity) and total neutron scattering length $\sum b$ (Table I). Intramicellar structures and intermicellar interactions for the same volume fraction are independent of the different SANS contrasts (e.g., there are no substantial isotope effects).

(ii) SLD distributions are calculated from the information given in Table I, following the incompressibility principle. In other words, $\rho=\sum b/\sum v$.

(iii) The micelle is spherical with a core-shell structure and polydispersity effects may be neglected.

The first postulate attributes the variations in the observed scattering patterns under the various contrast conditions to SLD differences. It follows that samples have the same intermicellar structure factor $S(q)$, independent of deuterium labeling, and that minor differences in molar volume, dielectric properties, etc., between the H and D species may be neglected. The third postulate allows us to represent $I_{expt}(q)$ as

$$I(q)=n_p|F(q)|^2S(q) \\ =n_pP(q)S(q)\ , \tag{1}$$

where $F(q)$ and $P(q)$ are the amplitude factor and particle form factor, respectively. Note that the latter function contains the scattering length density, so $P(0)\neq 1$, as in the case where the SLD differences are included in a separate "contrast factor."

$$n_p=[\phi/(v_{TMA}+v_{DS})-n_{CMC}]/N \tag{2}$$

is the number density of micelles and ϕ, v_{TMA}, v_{DS}, n_{CMC}, and N are the volume fraction of TMADS, the molecular volumes of TMA^+ and DS^-; the critical micelle concentration of TMADS, and the aggregation number, respectively.

For an isolated spherical ionic micelle including the surrounding ion cloud, $F(q)$ in Eq. (1) is expressed as

$$F(q)=4\pi\int_0^{R_c}\bar{\rho}(r)\frac{df(q,r)}{dr}dr\ , \tag{3}$$

where

$$f(q,r)=[\sin(qr)-qr\cos(qr)]/q^3\ , \tag{4}$$

$\bar{\rho}$ is a function of the distance from the center of a micelle r defined as

$$\bar{\rho}(r)=\rho(r)-\rho(R_c)\ , \tag{5}$$

and R_c is the radius (boundary) of a spherical cell at which a micelle is centered and is determined to equalize the micellar concentration of the practical system to that of the cell model

$$R_c=(3/4\pi n_p)^{1/3}\ , \tag{6}$$

The micellar structure of TMADS will be discussed here in terms of two models as follows.

B. Models for isolated micellar systems

1. The core shell ion-cloud model

As the most feasible model to describe the isolated micellar system, the core shell ion-cloud (CSI) model was introduced to analyze the obtained SANS data. The micellar particle in this model consists of three regions; core, shell, and ion cloud. This model gives the following SLD (ρ) distribution:

$$\rho(r)=\begin{cases}\rho_{C_{12}H_{25}} & (0\le r\le R_1)\\ \rho_{\text{shell}} & (R_1<r\le R_2)\\ \rho_{\text{ion cloud}}(r) & (R_2<r\le R_c).\end{cases} \tag{7}$$

The hydrophobic core is formed with N (the aggregation number) hydrocarbon chains of DS and its radius R_1 is given by

$$Nv_{C_{12}H_{25}}=4\pi R_1^3/3 \ . \tag{8}$$

It is assumed that all the hydrocarbon chains are confined within the core (radius R_1), which seems reasonable in view of the large hydrophobicity of alkyl chains. The core SLD is given in Table I. The shell region ($R_1<r\leq R_2$) consists of N head groups of DS^- (SO_4^-) and bound TMA^+, with hydrating water molecules occupying the remaining volume of the shell. Hence the SLD in the shell (ρ_{shell}) is given by

$$\rho_{shell}=[V_{sol}\rho_{sol}+(N-Z)b_{TMA}+Nb_{SO_4}]/V_{shell} \ , \tag{9}$$

where

$$V_{shell}=4\pi(R_2^3-R_1^3)/3 \tag{10}$$

is the shell volume and Z is the effective charge number of the micellar particle. b_{TMA} and b_{SO_4} are the molecular scattering lengths of TMA^+ and SO_4^-, respectively (Table I). V_{sol} is the volume occupied by the hydrating water molecules and is given as

$$V_{sol}=V_{shell}-(N-Z)v_{TMA}-Nv_{SO_4} \ . \tag{11}$$

Therefore, the hydration number per DS molecule w can be calculated as

$$w=V_{sol}/Nv_{sol} \ , \tag{12}$$

where v_{sol} is the molecular volume of water, ρ_{sol} is the ρ of the solvent and is given with the volume fraction of D_2O in D_2O-H_2O solvents ϕ_{D_2O} as

$$\rho_{sol}=\rho_{D_2O}\phi_{D_2O}+\rho_{H_2O}(1-\phi_{D_2O}) \ . \tag{13}$$

$\rho_{ion\ cloud}$ may be expressed as a function of r

$$\rho_{ion\ cloud}(r)=\rho_{sol}+(\rho_{TMA}-\rho_{sol})v_{TMA}n_{TMA}(r)+(\rho_{DS}-\rho_{sol})v_{DS}n_{DS}(r) \ , \tag{14}$$

where n_{TMA} and n_{DS} are the local concentration of TMA^+ and DS^- and follow the Poisson-Boltzmann equation for spherically symmetric systems [11]

$$\frac{1}{r^2}\frac{d}{dr}\left[r^2\frac{d\varphi(r)}{dr}\right]=-4\pi\lambda_B[n_{TMA}(r)-n_{DS}(r)]=-4\pi\lambda_B[n_{TMA0}e^{-\varphi(r)}-n_{DS0}e^{\varphi(r)}] \ . \tag{15}$$

φ is the electrostatic potential nondimensionalized by kT and satisfies the boundary conditions

$$\varphi(R_c)=0 \ , \tag{16}$$

$$\left.\frac{d\varphi}{dr}\right|_{r=R_2}=-\frac{Z\lambda_B}{R_2^2} \tag{17}$$

and

$$\lambda_B=e^2/4\pi\varepsilon kT \tag{18}$$

is the Bjerrum length. n_{TMA0} and n_{DS0} are the activities (the local concentrations where $\varphi=0$) of TMA^+ and DS^-, which are related to the mean concentrations $\overline{n_{TMA}}$ and $\overline{n_{DS}}$ by

$$\overline{n_{TMA}}=n_{TMA0}\langle e^{-\varphi}\rangle=n_{CMC}+Zn_p \ , \tag{19}$$

$$\overline{n_{DS}}=n_{DS0}\langle e^{\varphi}\rangle=n_{CMC} \ , \tag{20}$$

where $\langle\ \rangle$ represents the volume average. Hence the TMADS molecules that do not belong to micelle behave as added salt. By introducing the Poisson-Boltzmann condition in this manner, the SLD (ρ) distribution in the ion-cloud region is determined only by Z and R_2 over the whole range of surface potential. In summary, an isolated micellar system can be described by using only three variables N, R_2, and Z as fitting parameters.

2. *The core shell model*

The CSI model was also compared to the simple core shell model, which has previously been widely used [22–27] to analyze the micellar structure. In this model the SLD (ρ) is given as a step function

$$\rho(r)=\begin{cases}\rho_{C_{12}H_{25}} & (0\leq r\leq R_1)\\ \rho_{shell} & (R_1<r\leq R_2)\\ \rho_{soln} & (R_2<r\leq R_c),\end{cases} \tag{21}$$

where $\rho_{C_{12}H_{25}}$ and ρ_{shell} are the same as those in Eq. (8). ρ_{soln} is a constant given by

$$\rho_{soln}=\rho_{sol}+(\rho_{TMA}-\rho_{sol})v_{TMA}\overline{n_{TMA}}+(\rho_{DS}-\rho_{sol})v_{DS}\overline{n_{DS}} \ . \tag{22}$$

This model is based on the assumption that simple ions are distributed uniformly in the solvent.

C. Fitting procedure

$F(q)$ was calculated from both the above models and $S(q)$ was determined by

$$S_i(q)=I_{expt,i}(q)/n_pP_i(q) \ , \tag{23}$$

where the subscript i indicates the different contrast conditions 1–4. $I_{expt,i}(q)$ is the coherent experimental scattering intensity (cross section) from which solvent scattering and the incoherent background of the solute have been subtracted. In order to facilitate this subtraction, the (angle-independent) scattering of D_2O (≈ 0.06 cm^{-1}) was measured, along the flat backgrounds of H_2O (≈ 1.3 cm^{-1}) and various H_2O-D_2O mixtures (e.g., 0.605 cm^{-1} for a 1:1 mixture). In addition, a small correction (~ 0.015–0.025 cm^{-1}) was made for the incoherent scattering of the micelle (as opposed to the solvent). As an independent check on the efficiency of the background

subtraction it may be noted that both $I_{expt}(q)$ and $n_pP(q)$ should tend to zero at higher q ($0.14 < q < 0.15$ Å^{-1} for CC 1 and $q \sim 0.23$ Å^{-1} for CCs 2 and 3). From postulate (i), $S_i(q)$'s calculated by Eq. (23) are expected to give the same curve at all contrasts. Therefore the mutual curve fitting for 6-vol % series was carried out to minimize the deviation among the structure factors calculated with the three contrast conditions. For 3-vol % series, only the deviation between $S_2(q)$ and $S_3(q)$ was considered in the parameter fitting because of the poor statistics with the data collected for CC 1. All the fitting calculations were performed by using the super computer M-1800 (Fujitsu) in Kyoto University Data Processing Center.

D. Profile of the counterion distribution and structural parameters of the micelle

$I_{expt,i}(q)$ and $n_pP_i(q)$, which were fitted with the CSI model, under contrast conditions 1–3 at 6 vol % are shown in Fig. 1. The fitted variables and the other model parameters are listed in Table II. R_1 was calculated to be 18.6 Å from the N value (=77) with Eq. (8) and the shell thickness ($=R_2-R_1$) was estimated to be 4.6 Å. The aggregation number (N) obtained in this study was less than that reported in Ref. [24] ($\sim$94), although the inner radius R_1 estimated here was a little larger than that in Ref. [24] (=17.2 Å). This discrepancy probably arises from the different assumptions used to determine the core size. In Ref [24], a portion of the DS-hydrocarbon chain is located outside the core (in the shell region), whereas it is assumed to be confined to the core in this work. Thus the shell thickness estimated in Ref. [24] (11.5 Å) was much larger than that obtained in this study (4.8 Å). In addition, the shell thickness of a SDS micelle was estimated to be $\sim$11 Å, whereas calculations in Ref. [23] indicated a thickness $\sim$5–7.5 Å. This suggests that it is difficult to determine a certain structure of a micelle with too many fitting parameters.

Figure 3 shows the intermicellar structure factors derived from the three different contrast conditions for the 6-vol % series. $S_1(q)$, $S_2(q)$, and $S_3(q)$ are in excellent agreement, indicating the self-consistency of the analysis. Radial SLD (ρ) distributions for the (spherical) CSI model at the four ρ contrast conditions are shown in Fig. 4. These profiles were calculated from the fitted N, R_2, and Z with Eq. (7). From this figure, the largest fluctuation in ρ seems to arise from the hydrocarbon core region in D_2O (CCs 2 and 3). However, $n_pP_2(q)$ and $n_pP_3(q)$ are quite different in their absolute value and intersect each other at $q \sim 0.14$ Å^{-1} in Fig. 1(a). This tendency is observed also in $I_{expt,2}(q)$ and $I_{expt,3}(q)$. Of course, the ρ distribution at CC 1 is quite different from those at CCs 2 and 3 and results in $n_pP_1(q)$, whose shape deviates largely from $n_pP_2(q)$ and $n_pP_3(q)$. In contrast condition 1, ρ in the core ($\rho_{C_{12}H_{25}}$) and ρ in the bulk are nearly equal and the fluctuation in ρ is mainly due to the shell and the ion cloud. $n_pP_1(q)$ indicates the oscillating behavior, which is reflected in $I_{expt,i}(q)$.

Figure 5 shows $I_{expt,4}(q)$ and $n_pP_4(q)$, which were calculated from the ρ distributions at contrast condition 4 (Fig. 3). $I_{expt,4}(q)$ could not be used in the parameter fitting because of its low intensity and bad statistics. However, a product of $n_pP_4(q)$ and $S(q)$, which is defined as an average of $S_2(q)$ and $S_3(q)$, is also shown as $I_{theor,4}(q)$ in Fig. 5. $I_{theor,4}(q)$ reproduces the tendency of $I_{expt,4}(q)$ within the range of the statistical error.

Figure 2 shows $I_{expt,i}(q)$ and $n_pP_i(q)$ of 3-vol % series. The parameter fitted for this series are listed in Table II and they give similar values to those of 6 vol %. Therefore, the difference in shapes of $I_{expt,i}(q)$ from those of 6 vol % are mainly due to the difference in $S(q)$. S_i of 3-vol % series are shown in Fig. 6. These were calculated according to Eq. (23) and obtained by requiring that $S_2(q)$ and $S_3(q)$ coincide with each other. However, $S_1(q)$ agreed well with $S_2(q)$ and $S_3(q)$, although $S_1(q)$ had not been considered in the parameter fitting. These $S(q)$ showed the maximum at lower q than the 6-vol %

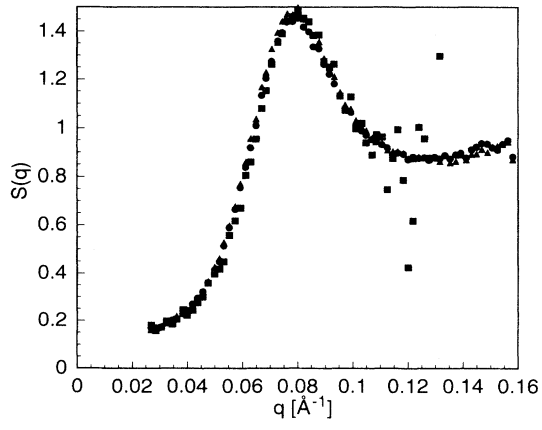

FIG. 3. Intermicellar structure factors $S(q)$ of 6-vol % samples plotted against q. The calculation is based on the CSI model. ■, ●, and ▲ indicate $S(q)$ at contrast conditions 1, 2, and 3, respectively.

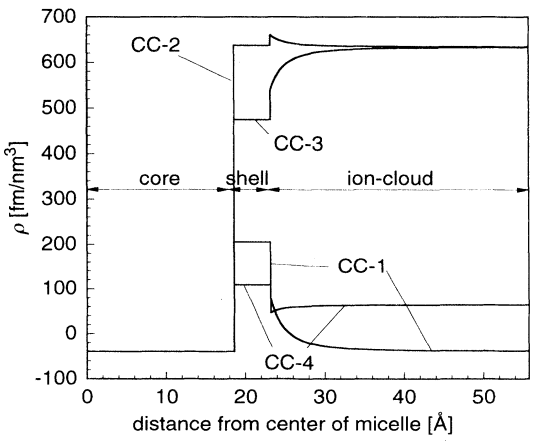

FIG. 4. Scattering length densities ρ of 6-vol % samples in the CSI model as functions of the distance from the center of a micelle r at four contrast conditions (see Table II).

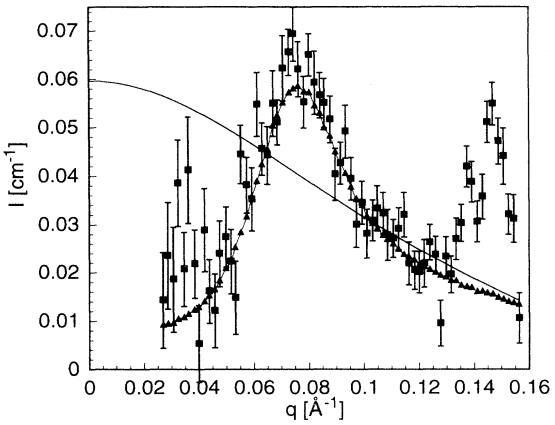

FIG. 5. $I_{\text{expt}}(q)$, $n_p P(q)$, and I_{theor} (■ with error bars, ——, and ▲, respectively) of a 6-vol % sample at contrast condition 4 plotted against q.

system corresponding to the decrease of n_p. The maximum value of $S(q)$ reaches 1.4, suggesting the strong electrostatic interaction between micelles. This is also consistent with the charge number ($Z=44$) and the large calculated value of the surface potential ($\varphi_s=-4.67kT$), as shown in Table II.

In this work, Z is the number of counterions dissociated from the hydrated shell of a micelle, rather than the activity number [33], which is the number of the counterions completely free from the electrostatic influence of macroions. Although the binding of TMA^+ into the micellar shell is not accompanied by any chemical process, a certain dissociation equilibrium is considered to be established at the surface. The local concentration of TMA^+ at the surface [$n_{TMA}(R_2)$ in Eq. (15)] was calculated to be $1.6M$ in the CSI model from the fitted parameters. With this value, an intrinsic dissociation constant of the Stern layer to TMA^+ was estimated as $2.1M$ for the 6% system.

φ_s [$=\varphi(R_2)$] was calculated to be much less than -4 (-100 mV) in the CSI model and indicates that it is not appropriate to describe the simple ion distribution according to the linear (Debye-Hückel) approximation; in such a case of large $|\varphi_s|$, the difference between the electrostatic potential calculated with this approximation and that calculated via nonlinear methods cannot be neglected and gives rise to different ion distributions. Thus, for such highly charged colloidal systems, it is necessary to take account of the interparticle interaction, which is strongly dependent on the simple ion distribution. For example, the Debye screening length κ^{-1} has often been used as an estimate of the range of the electrostatic force in macroionic systems by many researchers [9,10,34]. It is well known, however, that κ^{-1} should not be calculated with the mean concentrations of simple ions but with the *activities,* especially for highly charged systems. In this work, the counterion activity is expected to be less than 2% of the local concentration at the micellar surface whose value was estimated above and this results in a much larger value of κ^{-1} than that calculated via the mean concentration. Data from ultra-small-angle x-ray scattering exhibited an unexpected variation of the interparticle distance in colloid crystals with salt concentration [35]. These findings may be rationalized by using the κ^{-1} value calculated from the activity to show that the distance scales well with κa (a is the radius of the particle) [36].

The fitted parameters by the core-shell (CS) model are also listed in Table II. Both R_1 and R_2 were estimated to be larger than those with the CSI model at 6 vol % concentration. The goodness of fit of this model is almost the same as that of the CSI model and the volume fraction (or n_p) dependence of N reproduces the tendency reported in some papers [24] better than that with the CSI model. It should be emphasized, however, that the CS model is less feasible physically than the CSI model; counterions cannot be distributed uniformly in the system [10–14]. Figure 7 shows the ρ distribution in the CS

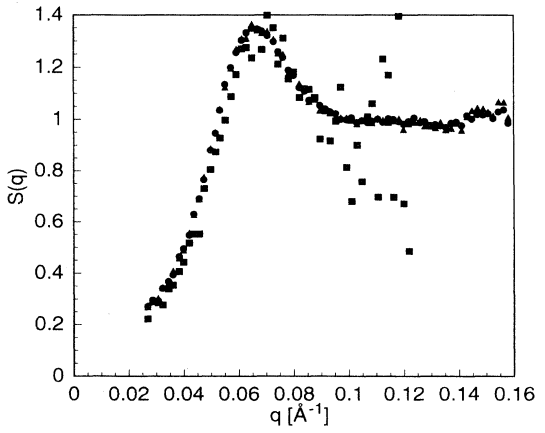

FIG. 6. $S(q)$ of 3-vol % samples plotted against q. Symbols are as in Fig. 3.

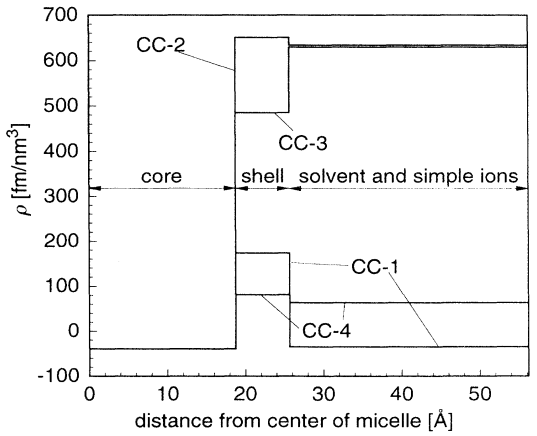

FIG. 7. Scattering length densities ρ of 6-vol % samples in the CS model as functions of r at four contrast conditions.

model at 6 vol %. Since the shell is defined to include the ion cloud in the CS model, this results in a much larger shell thickness than in the CSI model. The differences in the shell thickness between these two models suggests that the contribution of counterion cloud in the SANS intensities is detectable enough and that the simple core-shell model, which has often been widely used in the literature, may be inadequate when the scattering from counterions is dominant.

V. CONCLUSION

The counterion distribution around the highly charged spherical micelle of tetramethylammonium dodecylsulfate has been evaluated by SANS in combination with internal and external contrast variation technique. In all the steps of the analysis, we attempted to minimize the number of fitting parameters. Similarly, we avoided *a priori* calculations of the structure factor, from either the mean spherical approximation MSA [37] or the rescaled mean spherical approximation (RMSA) [38]. Not only would this have introduced additional fitting parameters, but also the $S(q)$, which is calculated from the interparticle potential function based on the Debye-Hückel approximation, is not reliable in cases where $|\varphi_s|$ is large. In fact, $|\varphi_s|$ was expected to exceed 4 in the CSI model. Hartland, Grieser, and White evaluated the surface potential of SDS micelles by spectroscopic probe measurements and reported its absolute value to be $3.8kT-5.7kT$ in the range of NaCl concentration $0.1M-0M$ [39]. Dunstan and White determined the ζ potential of SDS micelles to be $3.0kT-6.4kT$ by mobility measurements [40]. Even with the Z value estimated in Ref. [24] (~ 20), $|\varphi_s|$ should exceed 3 and the system will be beyond the Debye-Hückel approximation. In addition to the internal structure of a micelle, the simple ion distribution plays a very important role in determining the physico-chemical characteristics of the ionic micellar systems. Further research along these lines should contribute to our understanding of colloidal phenomena such as ordering, small-ion effect on diffusion and on electrophoresis.

ACKNOWLEDGMENTS

This work is supported by the U.S.–Japan Cooperative Program on Neutron Scattering, to which our sincere gratitude is due. Special thanks are to Dr. J. S. Lin (ORNL) for his kind support of SANS measurements at ORNL, which was supported by the Division of Materials Sciences, U.S. Department of Energy, under Contract No. DE-AC05-840R21400 with Martin Marietta Energy Systems Inc. H.M. expresses his deep thanks to the members of Solid State Division, ORNL, for their kind support and help during his stay in Oak Ridge. K.S. gratefully acknowledges the financial support of this work by the Japan Society for the Promotion of Science for Young Scientists.

[1] F. Oosawa, J. Polym. Sci. **23**, 421 (1957).
[2] G. S. Manning, J. Chem. Phys. **51**, 924 (1969).
[3] L. Kotin and M. Nagasawa, J. Chem. Phys. **36**, 873 (1962).
[4] M. Le Bret and B. H. Zimm, Biopolymers **23**, 271 (1984).
[5] M. Gueron and G. Weisbuch, J. Phys. Chem. **83**, 1991 (1979).
[6] M. Satoh, J. Komiyama, and T. Iijima, Macromolecules **18**, 1195 (1985).
[7] T. Alfrey, Jr., P. W. Berg, and H. Morawetz, J. Polym. Sci. **7**, 543 (1951).
[8] K. S. Schmitz, *Macroions in Solution and Colloidal Suspension* (VCH, Weinheim, 1993).
[9] E. J. W. Verwey and J. Th. G. Overbeek, *Theory of the Stability of Lyophobic Colloids* (Elsevier, Amsterdam, 1952).
[10] I. Sogami and N. Ise, J. Chem. Phys. **81**, 6320 (1984).
[11] S. Alexander, P. M. Chaikin, P. Grant, G. J. Morales, and P. Pincus, J. Chem. Phys. **80**, 5776 (1984).
[12] M. Fushiki, J. Chem. Phys. **97**, 6700 (1992).
[13] E. Sanchez-Sanchez and M. Lozada-Cassou, Chem. Phys. Lett. **190**, 202 (1992).
[14] T. Gilanyi, J. Colloid Interface Sci. **125**, 641 (1988).
[15] M. V. Smalley, Mol. Phys. **71**, 1251 (1990).
[16] I. S. Sogami, T. Shinohara, and M. V. Smalley, Mol. Phys. **76**, 1 (1992).
[17] P. J. W. Debye and E. Hückel, Phys. Z. **24**, 185 (1923).
[18] K. Sumaru, H. Matsuoka, and H. Yamaoka, J. Phys. Chem. **98**, 6771 (1994).
[19] C. F. Wu, S. H. Chen, L. B. Shih, and J. S. Lin, Phys. Rev. Lett. **61**, 645 (1988).
[20] C. F. Wu, S. H. Chen, L. B. Shih, and J. S. Lin, J. Appl. Cryst. **21**, 853 (1988).
[21] J. R. C. van der Maarel, L. C. A. Groot, J. G. Hollander, W. Jesse, M. E. Kuil, J. P. Cotton, G. Jannik, A. Lapp, and B. Farago, Macromolecules **26**, 7295 (1993).
[22] J. B. Hayter and J. Penfold, Colloid Polym. Sci. **261**, 1022 (1983).
[23] R. Triolo, E. Caponetti, and V. Graziano, J. Phys. Chem. **89**, 5743 (1985).
[24] S. S. Berr, M. J. Coleman, R. R. Marriott Jones, and J. S. Johnson, Jr., J. Phys. Chem. **90**, 6492 (1986).
[25] *Physics of Amphiphiles: Micelles, Vesicles and Microemulsions,* edited by V. Degiorgio and M. Corti (Italian Physical Society, Bologna, 1985).
[26] *Surfactant Solutions,* edited by R. Zana (Dekker, New York, 1987).
[27] *Surfactants in Solution,* edited by K. L. Mittel and D. Bothorel (Plenum, New York, 1986), Vol. 4.
[28] V. F. Sears, Neutron News **3**, 26 (1992).
[29] G. D. Wignall, in *The Physical Properties of Polymers,* edited by J. E. Mark (American Chemical Society, Washington, D.C., 1993), p. 313; G. D. Wignall, in *Encyclopedia of Polymer Science and Engineering,* 2nd ed., edited by M. Grayson and J. Kroschwitz (Wiley, New York, 1987), Vol. 10, p. 112.
[30] J. S. Higgins and H. Benoit, *Polymers and Neutron Scattering* (Oxford University Press, New York, 1994).
[31] W. C. Koehler, Physica B (Utrecht) **137**, 320 (1986).
[32] G. D. Wignall and F. S. Bates, J. Appl. Cryst. **20**, 28 (1987).

[33] N. Imai and K. Iwasa, Isr. J. Chem. **11**, 223 (1973).
[34] T. Okubo, J. Chem. Phys. **86**, 5182 (1987).
[35] H. Matsuoka, T. Harada, and H. Yamaoka, Langmuir **10**, 4423 (1994).
[36] H. Matsuoka, T. Harada, K. Kago, and H. Yamaoka (unpublished).
[37] J. B. Hayter and J. Penfold, Mol. Phys. **42**, 109 (1981).
[38] J.-P. Hansen and J. B. Hayter, Mol. Phys. **46**, 651 (1982).
[39] G. V. Hartland, F. Grieser, and L. R. White, J. Chem. Soc. Faraday Trans. 1 **83**, 591 (1987).
[40] D. E. Dunstan and L. R. White, J. Colloid Interface Sci. **134**, 147 (1990).